Right band gaps for the right reason at low computational cost with a meta-GGA

Timo Lebeda [1,2] Thilo Aschebrock,[1] Jianwei Sun,[2] Linn Leppert,[3] and Stephan Kümmel [1,*]

[1]*Theoretical Physics IV, University of Bayreuth, 95440 Bayreuth, Germany*

[2]*Department of Physics and Engineering Physics, Tulane University, New Orleans, Louisiana 70118, USA*

[3]*MESA+ Institute for Nanotechnology, University of Twente, 7500 AE Enschede, The Netherlands*

(Received 4 February 2023; revised 15 June 2023; accepted 22 August 2023; published 19 September 2023)

In density functional theory, traditional explicit density functionals such as the local density approximation and generalized gradient approximations cannot accurately predict the band gap of solids for a fundamental reason: They lack the exchange-correlation derivative discontinuity. By comparing Kohn-Sham and generalized Kohn-Sham calculations, we here show that the nonempirical meta-generalized-gradient-approximation (meta-GGA) TASK from Aschebrock and Kümmel [Phys. Rev. Res. **1**, 033082 (2019)] predicts the right gaps for the right reason, i.e., as a combination of a proper Kohn-Sham gap and a substantial derivative discontinuity contribution. For many materials from small-gap semiconductors to large-gap insulators, the proper band gap is thus obtained. We further study a group of metal-halide perovskites for which the band gap is notoriously hard to predict. For these materials, TASK yields band gaps very similar to the nonlocal screened hybrid Heyd-Scuseria-Ernzerhof functional, yet at a fraction of the hybrid functional's computational cost. We discuss the influence of correlation functionals, and open questions in the comparison of calculated band gaps with experimental ones.

DOI: 10.1103/PhysRevMaterials.7.093803

I. INTRODUCTION

The discovery of new materials is key for many applications [1] such as the next generation of solar modules [2–4], catalysts with improved efficiency [5], or batteries for energy storage [6,7]. For the computational screening of new materials, numerically efficient methods are required that predict material properties with sufficient accuracy [7–9]. Density functional theory (DFT) is very popular for such electronic structure calculations due to its balance between useful accuracy and reasonable computational cost. An example for an ongoing materials discovery quest is the search for nontoxic, earth-abundant, and stable semiconductors that can serve as light-converting materials in a wide range of applications. Metal-halide perovskites are a broad family of materials with outstanding chemical and electronic diversity that have received a lot of attention because of their versatile and highly tunable material properties [10–13]. The quintessential metal-halide perovskite, methylammonium (MA) lead iodide ($CH_3NH_3PbI_3$), e.g., has been used in solar cells with certified power conversion efficiencies exceeding 26% [14]. Since the family of metal-halide perovskites comprises thousands of stable materials [15,16], material-selection procedures have to be based on suitable criteria. The band gap is one of the most important properties for high-throughput material discovery and should be slightly larger than 1 eV for single-junction solar cells as a consequence of the detailed-balance limit [17]. Predicting the band gaps of perovskites with a reasonable reliability, yet at the same time low computational cost such that many materials can be computationally screened, is therefore an important task.

The (fundamental) band gap E_g of a system with N electrons is defined by

$$E_g = I(N) - A(N), \tag{1}$$

where $I(N)$ is the ionization potential and $A(N)$ is the electron affinity of the N-electron system, respectively. In a DFT calculation within the Kohn-Sham scheme, the band gap splits [18,19] into the Kohn-Sham gap Δ_{KS} and the exchange-correlation (xc) derivative discontinuity Δ_{xc},

$$E_g = I(N) - A(N) = \Delta_{KS} + \Delta_{xc}. \tag{2}$$

The Kohn-Sham gap

$$\Delta_{KS} = \varepsilon_{LU}^{KS} - \varepsilon_{HO}^{KS} \tag{3}$$

stems from the orbital-dependent kinetic energy [20] and is the difference between the lowest unoccupied (LU) and the highest occupied (HO) one-electron energy. For occupation numbers that respect the Aufbau principle, it is always nonnegative [21].

The xc derivative discontinuity on the other hand vanishes for density functional approximations that explicitly depend only on the density, or quantities directly derived from it, e.g., its spatial derivatives [18,22–26]. Therefore the local density approximation (LDA) [27] and generalized gradient approximations (GGAs) [28,29] severely underestimate the band gaps of semiconductors and insulators. The comparison with Green's-function-based quasiparticle calculations has led to the estimate that the xc derivative discontinuity often is responsible for 30–50 % or more of the band gap [30,31], and recent reconstructions of the exact Kohn-Sham system

*stephan.kuemmel@uni-bayreuth.de

for solids have confirmed the substantial contribution that Δ_{xc} makes to the gap [32].

Within the Kohn-Sham scheme, Δ_{KS} would not generally correspond to the fundamental gap even for the unknown exact xc functional [22,30,32–35]. However, for orbital-dependent functionals, the generalized Kohn-Sham formalism offers an attractive alternative [36]. In generalized Kohn-Sham theory the potential is no longer multiplicative. Depending on the xc approximation used, it leads to a set of orbital-dependent differential (meta-GGA) or integral (exact exchange) operators. This allows one to strive for xc approximations where the eigenvalue gap of the generalized partially interacting reference system equals the fundamental gap, i.e., for which

$$\Delta_{gKS} = \varepsilon_{LU}^{gKS} - \varepsilon_{HO}^{gKS} = E_g. \tag{4}$$

This is exploited, for example, in the range-separated hybrid Heyd-Scuseria-Ernzerhof functional (HSE) [37,38], where the short-range–long-range splitting parameter is used to empirically find a good generalized Kohn-Sham system. A more sophisticated choice of the generalized Kohn-Sham system is made in the optimally tuned range-separated hybrids [39,40], where a system-dependent parameter is fixed by enforcing the ionization potential (IP) theorem [41] for the N and $N+1$ electron systems as closely as possible. This tuning amounts to choosing the generalized Kohn-Sham system which minimizes Δ_{xc} [40,42,43] and aims for $\Delta_{gKS} = E_g$.

Comparison of Eqs. (2) and (4) shows that for a given xc functional, the difference between the generalized Kohn-Sham gap and the Kohn-Sham gap equals the xc derivative discontinuity,

$$\Delta_{xc} = \Delta_{gKS} - \Delta_{KS}. \tag{5}$$

Note that Eq. (5) only holds under the assumption that the orbitals do not change when switching from the Kohn-Sham to a generalized Kohn-Sham formalism. The latter is at least true in perturbation theory to first order [44].

In the past, local multiplicative potentials were constructed yielding a Kohn-Sham gap that closely approximates the fundamental gap [45,46]. These constructions, however, lead to other problems, e.g., divergences [47,48], too narrow bands [49], the lack of an energy functional and therefore, e.g., no prediction of bond lengths [45], a rather poor description of energetic binding [50], and numerical issues [51]. In the light of Eq. (2), one might interpret these issues as reflections of intrinsic inconsistencies that result when trying to map the effects of the nonlocal Δ_{xc} into a local potential.

Meta-generalized-gradient-approximations (meta-GGAs) [52–61] that depend on the kinetic energy density τ, and thus on the occupied Kohn-Sham orbitals, can have a nonvanishing xc derivative discontinuity [61–63], because the orbitals are implicit, nonlocal functionals of the density. Thus meta-GGAs in principle can improve band-gap prediction when evaluated in a generalized Kohn-Sham scheme [63,64]. In practice, however, the derivative discontinuity of many meta-GGAs is relatively small [62,63,65], so that the band gaps are not quantitatively accurate.

Therefore, so far functionals used for band-gap prediction typically include exact exchange [38,39,66,67] and thus come at a computational expense much larger than an LDA or GGA calculation. As a consequence, they have rarely been used for computationally demanding applications such as extensive materials screening. Because meta-GGAs have semilocal computational costs, they are the natural choice for large-scale calculations, provided they achieve the desired accuracy. Therefore understanding the nature of the xc derivative discontinuity in meta-GGAs and how it relates to the prediction of band gaps is a topic of substantial current interest [61,63,68–70].

In this paper, we show that the TASK meta-GGA from Aschebrock and Kümmel [61] yields the right band gaps for the right reason, namely by incorporating a substantial contribution from the derivative discontinuity on top of a Kohn-Sham gap with a magnitude similar to exact Kohn-Sham gaps.

II. GENERATING A SIZABLE DERIVATIVE DISCONTINUITY IN META-GGAS

The meta-GGAs that we study here [71] depend on the electron density n, its gradient ∇n, and the (positive) noninteracting kinetic energy density

$$\tau = \frac{\hbar^2}{2m} \sum_{\sigma} \sum_{i=1}^{N_\sigma} |\nabla \varphi_{i\sigma}|^2. \tag{6}$$

In the single-orbital limit, the kinetic energy density tends to the von Weizsäcker kinetic energy density

$$\tau_W = \frac{\hbar^2}{8m} \frac{|\nabla n|^2}{n}, \tag{7}$$

while in the uniform-density limit it becomes

$$\tau_{unif} = \frac{3\hbar^2}{10m} (3\pi^2)^{2/3} n^{5/3} =: A_s n^{5/3}. \tag{8}$$

The exchange energy is typically parametrized in dimensionless quantities that have a physical interpretation in certain limits. Here, we consider the reduced density gradient

$$s^2 = \frac{1}{4(3\pi^2)^{2/3}} \frac{|\nabla n|^2}{n^{8/3}}, \tag{9}$$

which can be used to detect noncovalent interactions [72], and the iso-orbital indicator

$$\alpha = \frac{\tau - \tau_W}{\tau_{unif}}, \tag{10}$$

which tends to zero in the iso-orbital limit, to one in the uniform-density limit, and to infinity in regions dominated by density overlap between closed shells [73]. Thus the meta-GGA exchange energy of a spin-unpolarized system reads

$$\begin{aligned} E_x^{mGGA} &= \int e_x^{mGGA}(n, \nabla n, \tau) d^3r \\ &= A_x \int n^{\frac{4}{3}} F_x^{mGGA}(s^2, \alpha) d^3r \end{aligned} \tag{11}$$

with the (exchange) enhancement factor $F_x^{mGGA}(s^2, \alpha)$ and $A_x = -(3e^2/4)(3/\pi)^{1/3}$. To obtain the exchange energy of a spin-polarized system, the exact spin scaling relation [74] can be applied to Eq. (11). The correlation energy is often defined via the (correlation) energy density per particle ε_c. For a direct comparison between exchange and correlation,

the enhancement factor of correlation over LDA exchange is defined as

$$E_c^{\mathrm{mGGA}} = \int n\varepsilon_c^{\mathrm{mGGA}}(n, \nabla n, \tau)d^3r =: A_x \int n^{\frac{4}{3}} F_c^{\mathrm{mGGA}}(r_s, s^2, \alpha)d^3r, \quad (12)$$

where the correlation enhancement factor, in addition to the dependence on s and α, depends on the Seitz radius $r_s = (4\pi n/3)^{-1/3}$. Typically, it also depends on a quantity for modeling the spin dependence, e.g., the spin polarization $\zeta = (n_\uparrow - n_\downarrow)/(n_\uparrow + n_\downarrow)$, but we have suppressed the spin dependence here for ease of notation.

It is well established that the xc derivative discontinuity is an important feature of the exact functional [18–20,75]. It was already discussed 40 years ago in the context of the straight line condition of Perdew, Parr, Levy, and Balduz [20], which states that the total energy as a function of the (fractional) particle number consists of straight lines between integer particle numbers. At integer particle numbers, however, the total energy has a kink, corresponding to a jump in its derivative. This derivative discontinuity with respect to the particle number equals the fundamental band gap of a solid,

$$E_g = \left.\frac{\partial E}{\partial N}\right|_+ - \left.\frac{\partial E}{\partial N}\right|_-, \quad (13)$$

where $|_-$ and $|_+$ denote derivatives evaluated on the electron-deficient and electron-rich side of the integer particle number. On the right-hand side, all energy contributions that are continuous in the density do not contribute. Thus

$$E_g = \underbrace{\left(\left.\frac{\delta T_s[n]}{\delta n(\mathbf{r})}\right|_+ - \left.\frac{\delta T_s[n]}{\delta n(\mathbf{r})}\right|_-\right)}_{\Delta_{\mathrm{KS}}} + \underbrace{\left(\left.\frac{\delta E_{xc}[n]}{\delta n(\mathbf{r})}\right|_+ - \left.\frac{\delta E_{xc}[n]}{\delta n(\mathbf{r})}\right|_-\right)}_{\Delta_{xc}}, \quad (14)$$

where the discontinuity originating in the noninteracting kinetic energy equals the Kohn-Sham gap of Eq. (3), and the second term is the derivative discontinuity of the exchange-correlation energy. In a meta-GGA, the latter is due to the orbital dependence of E_{xc}. Consequently, the xc derivative discontinuity of a meta-GGA reads

$$\Delta_{xc}^{\mathrm{mGGA}} = \int \frac{\partial e_{xc}}{\partial \tau}(\mathbf{r}')\left[\left.\frac{\delta \tau(\mathbf{r}')}{\delta n(\mathbf{r})}\right|_+ - \left.\frac{\delta \tau(\mathbf{r}')}{\delta n(\mathbf{r})}\right|_-\right]d^3r'. \quad (15)$$

To obtain further insight, one can simplify this expression by approximating the first term by its average over an "energetically important region,"

$$\frac{\partial e_{xc}}{\partial \tau} \approx \overline{\frac{\partial e_{xc}}{\partial \tau}}. \quad (16)$$

This derivation has been used in the construction of the TASK functional for exchange [61], and here we underpin it with additional considerations. The "energetically important region" denotes the spatial region in which the dominant contributions to the above integral emerge. The accuracy of this approximation may vary from system to system and especially between solids and molecules. Still, it provides useful insights into how an xc derivative discontinuity of desired sign and size can be generated.

The approximation of Eq. (16) allows one to pull the approximated term in front of the integral. Since the noninteracting kinetic energy density τ integrates to the usual noninteracting kinetic energy functional T_s, this leads to

$$\Delta_{xc}^{\mathrm{mGGA}} \approx \overline{\frac{\partial e_{xc}}{\partial \tau}}\Delta_{\mathrm{KS}}. \quad (17)$$

This implies that the xc derivative discontinuity of a meta-GGA is approximately proportional to the Kohn-Sham gap—if the approximation of Eq. (16) is justified. When one goes beyond this approximation, then there is the possibility for a nonvanishing xc discontinuity despite a vanishing Kohn-Sham gap. We discuss such a case (CdO) below. Within the approximation, the sign as well as the size of the xc derivative discontinuity can be controlled via the proportionality factor $\overline{\partial e_{xc}/\partial \tau}$, since the Kohn-Sham gap is non-negative.

It has been conjectured that the total xc derivative discontinuity as well as that of exchange must be positive in electronic systems. These conclusions have been based on, e.g., the numerical evidence that typical semilocal functionals (LDA and GGAs) systematically underestimate band gaps of solids [32] and explicit calculations of Δ_x and Δ_{xc} [76–80], as well as the observation that the ground-state energy as a function of particle number is concave upwards for systems with repulsive interactions. Because the exchange contribution to the xc derivative discontinuity, Δ_x, is typically much larger than that from correlation, we first consider exchange. A detailed discussion of the contribution from correlation follows in Sec. V.

To obtain a positive exchange derivative discontinuity, the proportionality condition equation (17) implies that one has to construct the meta-GGA exchange energy such that

$$\frac{\partial e_x}{\partial \tau} > 0 \quad (18)$$

in the energetically important region. Moreover, the magnitude of $\partial e_x/\partial \tau$, together with the Kohn-Sham gap, determines the size of Δ_x. For a parametrization of the exchange enhancement factor F_x in s and α the condition of Eq. (18) is equivalent to the condition [61]

$$\frac{\partial F_x}{\partial \alpha} < 0. \quad (19)$$

Thus there is a construction principle for the meta-GGA enhancement factor by which one can control the sign as well as the size of the exchange (x) or exchange-correlation (xc) derivative discontinuity.

III. RIGHT BAND GAPS FOR THE RIGHT REASON

In the following, we show that this construction principle indeed leads to the proper prediction of band gaps. In the context of this discussion, it is helpful to have in mind some general aspects of band-gap calculations. First, one must be aware that the calculated gaps depend on the lattice parameters and on numerical choices such as the size of the basis set, whether a pseudopotential is used or not, and possibly the details of the employed pseudopotential. Second, relativistic effects can influence the band structure of some materials noticeably. Third, the xc approximation influences the band

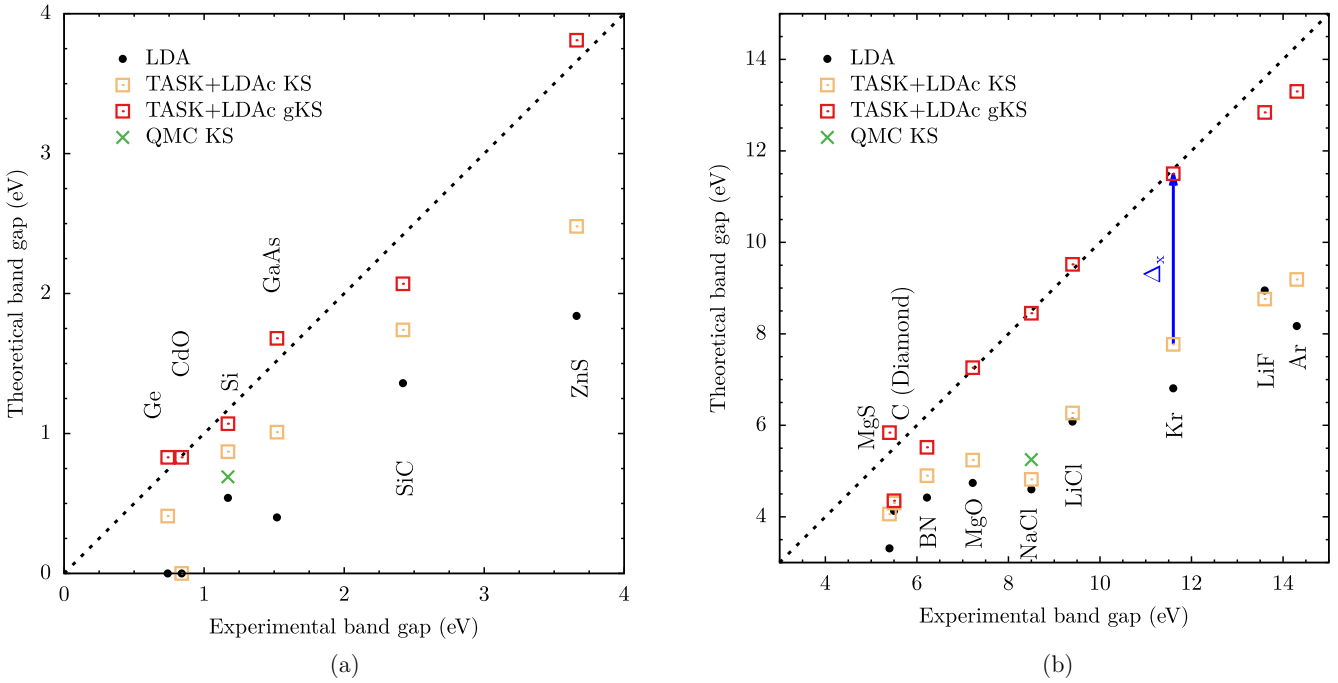

FIG. 1. Calculated vs experimental band gaps of (a) small-gap systems and (b) large-gap systems. The difference between the generalized Kohn-Sham (gKS) gaps and the Kohn-Sham (KS) gaps shows the exchange derivative discontinuity, illustrated for Kr by a blue arrow. Experimental bond lengths and experimental band gaps have been chosen as in Ref. [61] for all systems except NaCl. The bond length and reference value of NaCl are taken from Ref. [32] to allow for comparison with the QMC data. The green crosses mark the QMC-derived Kohn-Sham gaps of Si (0.69 eV) and NaCl (5.25 eV) from Ref. [32]. The dotted line illustrates exact agreement with the reference values.

structure via the single-particle gap and possibly the derivative discontinuity. Fourth and finally, for orbital-dependent xc approximations, it can make an important difference whether one is using the Kohn-Sham or the generalized Kohn-Sham scheme. In the Supplemental Material [81] we discuss these different aspects and show, e.g., in Tables SII and SIII, results for different density functionals and different levels of taking into account relativistic effects. In this paper, our focus is on the above-discussed meta-GGA construction principle.

The TASK meta-GGA for exchange [61] adheres to this principle and combines it with the fulfillment of nonempirical exact constraints. A correlation functional to go along with TASK is the iso-orbital corrected correlation (CC) [82]. It is based on the local spin density approximation (LSDA) in the parametrization of Perdew and Wang [83]. For systems without spin polarization, such as the solids in the test set studied below, the CC is identical to the LSDA correlation. In the following, we just write "TASK" to refer to TASK exchange with LSDA correlation to simplify the notation.

The decisive step for disentangling the single-particle contribution and the derivative discontinuity contribution to the band gap is to compare the gaps obtained within the Kohn-Sham scheme with those obtained from the generalized Kohn-Sham scheme; cf. Eq. (5) [84]. This logic has already been followed in Ref. [63]. Additionally, we compare the Kohn-Sham gaps of TASK with those of the LDA and with very recent quasiexact Kohn-Sham gaps obtained by inversion of highly accurate quantum Monte Carlo (QMC) ground-state densities [32].

We have performed all calculations using the BAND code [85–91] of the Amsterdam Modeling Suite. To this end, we have implemented an optimized effective potential (OEP) routine for TASK, using the Krieger-Li-Iafrate (KLI) approximation [92]. The Supplemental Material [81] lists the numerical details. It has previously been reported that the OEP routine for meta-GGAs in BAND needs an extremely fine (radial) Becke grid [63]. Our calculations with the TASK functional did not need this fine grid; cf. Sec. VI and the Supplemental Material [81]. Our experience that TASK [with both LDA correlation (LDAc) and CC] is numerically stable and efficient is in line with several very recent numerical stability analyses [93–95], which conclude that the numerical stability of TASK is on par with that of the Perdew-Burke-Ernzerhof functional (PBE) [96].

Figure 1 shows the computed band gaps compared with the experimental reference values for small-gap [i.e., smaller than 4 eV; Fig. 1(a)] and large-gap [i.e., larger than 4 eV; Fig. 1(b)] systems. On the one hand, the figure confirms the previous finding [61] that TASK evaluated in the generalized Kohn-Sham scheme predicts band gaps reliably for a large variety of systems. Especially for large-gap systems, which are very challenging for many other methods [69], TASK predicts the band gap quite accurately. The same trend has very recently been observed in a comprehensive study on the impact of the exchange enhancement factor on band gaps [70].

An important insight going beyond Ref. [61], on the other hand, emerges when looking at the Kohn-Sham gaps of TASK. The figures show that these Kohn-Sham gaps are close to or slightly larger than the gaps from LDA. Comparison of the Kohn-Sham and the generalized Kohn-Sham gaps thus demonstrates that the accurate prediction of the band gaps with TASK is *not* obtained by incorrectly open-

ing large Kohn-Sham gaps. Instead, TASK correctly includes a substantial contribution from the derivative discontinuity, which here stems from the TASK exchange. The difference between the generalized Kohn-Sham gap and the Kohn-Sham gaps indicates the derivative discontinuity, as highlighted for the example of Kr by the blue arrow in Fig. 1. One sees that here, $\Delta_x \approx 3.7$ eV, i.e., the discontinuity is responsible for about a third of the gap.

For most small-gap semiconductors, the fact that TASK achieves larger gaps than LDA can be attributed to two effects: First, the Kohn-Sham gaps are larger than those of the LDA, closing about half of the difference with respect to experiment. The remaining difference is then closed by the derivative discontinuity contribution that is included in the generalized Kohn-Sham eigenvalue gap. The situation is different for the large-gap systems. There, the relative increase of the TASK Kohn-Sham gaps over the LDA gaps is much smaller. This trend is in line with the accurate QMC-derived Kohn-Sham gaps from Ref. [32]: Also for the quasiexact Kohn-Sham gaps, the relative increase compared with the LDA gaps is larger for the small-gap system Si than for the large-gap system NaCl. Furthermore, also in terms of the absolute magnitude, the QMC-derived gaps support the meta-GGA results, as similar Kohn-Sham gaps are found in both approaches. The meta-GGA generalized Kohn-Sham gaps, on the other hand, are much larger and close to the experimental band gaps.

These results thus demonstrate that the meta-GGA predicts the right band gaps for the right reason: TASK does not require that the Kohn-Sham gap be spuriously opened up to match the experiment, but instead yields a Kohn-Sham gap that is somewhat larger than the LDA gap yet still of similar magnitude. It combines the Kohn-Sham gap with a substantial contribution from the derivative discontinuity to reach a band gap close to the experimental one. The high accuracy of the meta-GGA generalized Kohn-Sham gaps attests the usefulness of the construction principle of Eq. (19).

As a side remark, and in view of Sec. VI, we note that we also compared the band gaps obtained with TASK with the ones obtained with the HSE functional. The corresponding data are shown in Table SIV of the Supplemental Material. It shows that (with the exception of diamond, see below), TASK and HSE yield similar results for systems with gaps of up to ∼5 eV, whereas TASK yields larger gaps than HSE for systems with larger band gaps, in agreement with experiment.

IV. ENERGETICALLY IMPORTANT REGIONS IN DIFFERENT TYPES OF SYSTEMS

The trends described in the previous section hold for the large majority of systems. However, it is worthwhile to discuss the concept of averaging over the "energetically important region" [cf. Eq. (16)] in greater detail, because there are two interesting exceptions in our set of data. The first one is diamond, where we observe a rather large deviation of the TASK generalized Kohn-Sham gap from the experimental band gap. TASK enhances the Kohn-Sham gap of diamond only marginally compared with LDA, and the derivative discontinuity is insignificant. At least as remarkable is CdO. There, the Kohn-Sham gap of TASK vanishes like that of LDA, but the generalized Kohn-Sham gap is nevertheless in very good agreement with the experimental data.

These effects must have their origin in the electronic structure. In order to understand what is special about these two systems, we analyze their electronic structure in comparison to other materials. For this comparison we chose as one reference Ge, because its band gap is of very similar magnitude to the one of CdO and its lattice structure is similar to the one of diamond. As a second reference we chose NaCl, as its lattice structure is similar to the one of CdO and the QMC reference value is available. In the Supplemental Material we also discuss Si as a third natural reference system.

Figure 2 shows the electronic structure parameters r_s, s, and α, which enter the meta-GGA as the input, as well as the enhancement factor of TASK and (minus) its derivative with respect to α for Ge and C (diamond), and NaCl and CdO in Figs. 2(a) and 2(b), respectively. The input parameters are taken from a self-consistent TASK calculation in BAND. From these, we calculate $F_{\rm xc}^{\rm TASK}$ and $-\partial F_{\rm xc}^{\rm TASK}/\partial\alpha$ and finally plot all quantities along a path in the unit cell as indicated in the caption.

First, we compare Ge and diamond. Both systems are covalently bonded and have a diamond cubic lattice, so one might expect that they are similarly well described. However, Fig. 1 shows that for Ge the derivative discontinuity $\Delta_{\rm xc}$ is responsible for about half of the experimental gap, while it nearly vanishes for diamond. It is not obvious where this difference comes from; therefore we take a closer look at the electronic structure. Figure 2(a) shows that in both systems, $\partial F_{\rm xc}^{\rm TASK}/\partial\alpha$ has a similar magnitude everywhere except for the core region and the bonding region, where we define the bonding region as the central region between the nuclei with the shortest core-core distance, as denoted in Fig. 2. The core region, however, is unlikely to contribute significantly to $\Delta_{\rm xc}$. In the bonding region the magnitude of $\partial F_{\rm xc}^{\rm TASK}/\partial\alpha$ is approximately a factor of 2 larger for Ge than for diamond, as seen in the insets in Fig. 2(a). This is a relevant observation in view of Eq. (19): A more negative $\partial F_{\rm xc}^{\rm TASK}/\partial\alpha$ leads to a larger derivative discontinuity. Therefore we conclude that the bonding region is very important for these strongly bound systems, i.e., the bonding region makes a large part of the energetically important region in the sense of Eqs. (15) and (16). The reason for the different values of $\partial F_{\rm xc}^{\rm TASK}/\partial\alpha$ is the different values of α in the bonding region. In the bonding region of diamond, α takes rather small values down to $\alpha \approx 0.2$, while in Ge, as well as in NaCl and CdO, α is larger than 0.4 everywhere (except for the core region). However, for $\alpha \approx 0.2$, TASK has much less α-derivative than for larger values of α; cf. Fig. 3. Furthermore, in diamond the density in the bonding region is larger, i.e., r_s is smaller than for Ge, and this also reduces the derivative discontinuity because $\partial e_{\rm xc}/\partial\tau \propto n^{-1/3}\partial F_{\rm xc}/\partial\alpha \propto r_s\partial F_{\rm xc}/\partial\alpha$. Thus, in the case of diamond, the chosen parametrization of the TASK functional does not sufficiently pick up the energetically important region.

Next, let us compare Ge and CdO. Ge and CdO have a similar experimental band gap, and TASK predicts similar generalized Kohn-Sham gaps for both. However, TASK predicts a vanishing Kohn-Sham gap for CdO, while for Ge the predicted Kohn-Sham gap is of the magnitude that one

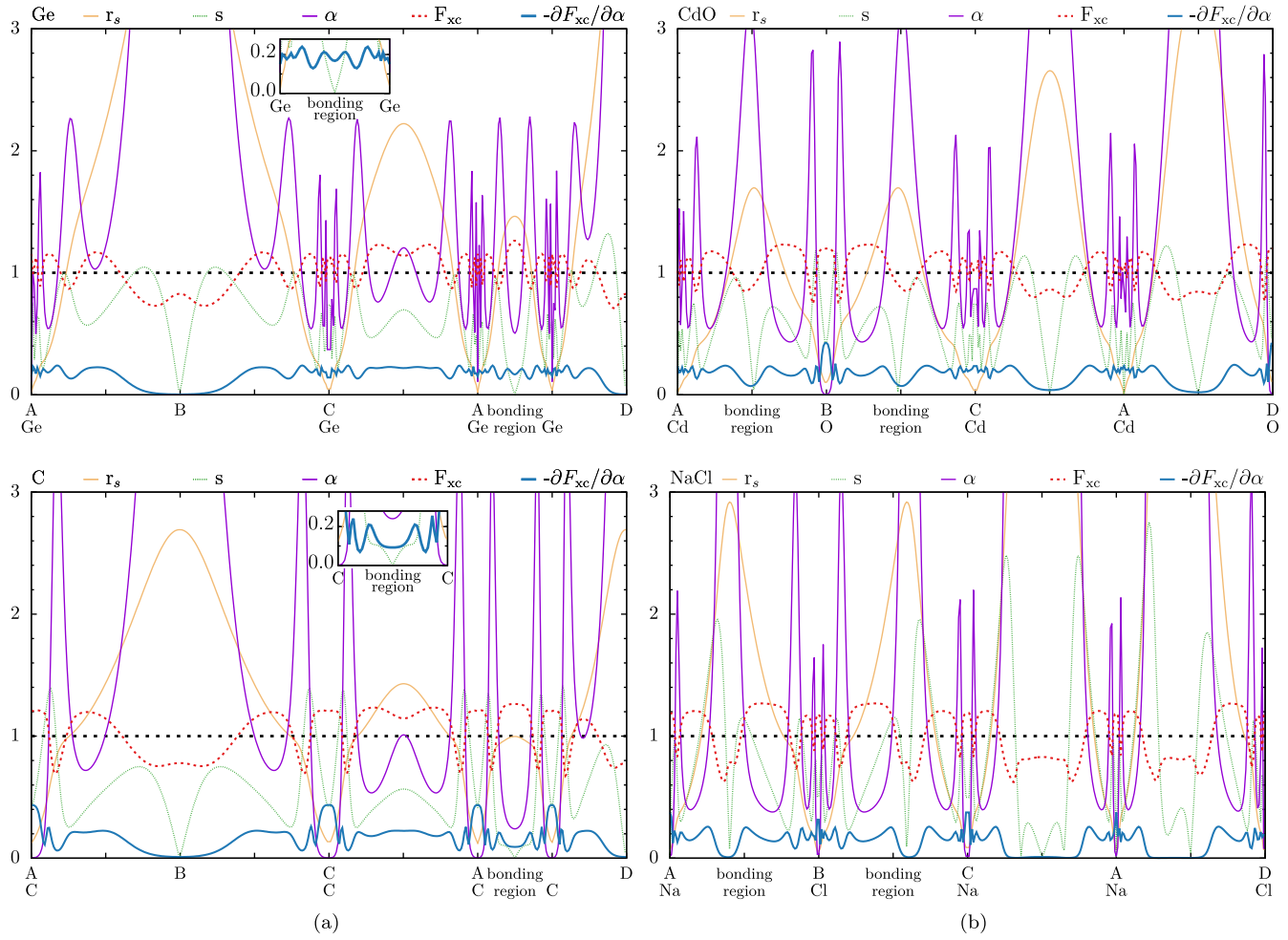

FIG. 2. The values of the Seitz radius r_s, the reduced density gradient s, and the iso-orbital indicator α along a path in the unit cell. (a) Ge and C in the diamond cubic structure. (b) NaCl and CdO in the rock-salt cubic structure. All values are calculated self-consistently with TASK in BAND [91]. Based on these values, the TASK enhancement factor F_{xc} and its derivative with respect to α, $\partial F_{xc}/\partial\alpha$, are calculated. The path is defined as $A \to B \to C \to A \to D$, where $A = (0, 0, 0)$, $B = (0, 0, \frac{1}{2})$, $C = (0, \frac{1}{2}, \frac{1}{2})$, and $D = (\frac{1}{2}, \frac{1}{2}, \frac{1}{2})$ (fractional coordinates with respect to lattice vectors). Along the path, the positions of the nuclei and the bonding region are indicated. The insets for Ge and C show a zoomed version of the bonding region. Note that the plots show the negative of $\partial F_{xc}/\partial\alpha$.

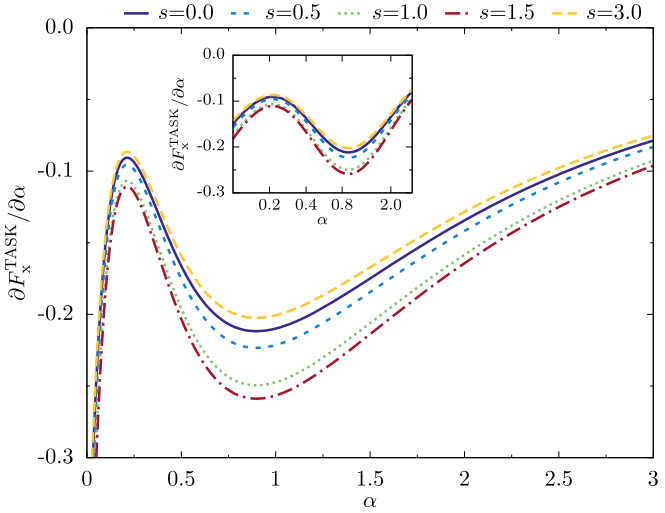

FIG. 3. Derivative of the TASK (exchange) enhancement factor F_x^{TASK} with respect to α as a function of α for different values of s. The inset has a logarithmic x axis.

expects for such semiconductors [30,32,34]. Figure 2 reveals the obvious substantial differences between Ge and CdO as a consequence of their different crystal structures. While Ge is in the diamond cubic structure, CdO is in the rock-salt cubic structure, like NaCl. This reflects their different bonding types: Ge and diamond are covalently bound, while CdO and NaCl are ionic crystals. Therefore a Kohn-Sham gap close to the (vanishing) LDA Kohn-Sham gap for CdO—and consequently, a larger contribution from the derivative discontinuity—is in line with the discussion in the previous section: There, we already observed that the difference between the Kohn-Sham gaps of LDA and TASK is different for ionic crystals and covalently bound crystals.

For the ionic crystals NaCl and CdO, it is not as clear as for the covalently bound systems what the energetically important region is. While the size of the Kohn-Sham gap of TASK in NaCl corresponds to about two-thirds of the size of the experimental gap, which is the right order of magnitude as confirmed by the QMC-derived Kohn-Sham gap, TASK predicts a vanishing Kohn-Sham gap for CdO. Still, the gen-

eralized Kohn-Sham gap of TASK matches the experimental value quite accurately in both systems. From Fig. 2, we observe that in a large part of the bonding region, $\partial F_{\rm xc}^{\rm TASK}/\partial\alpha$ nearly vanishes in NaCl and is small in CdO. This suggests that in the ionic crystals the bonding region is not as important for the gap as it is in the covalently bound semiconductors. Instead, the inner valence region, and possibly the core-valence region, become more important. (Here we define the inner valence region in the following way: Starting from the point where the reduced density gradient s has a minimum between two nuclei, go in the direction of one of the neighboring nuclei towards the highest maximum of s. The inner valence region starts at this maximum and reaches to the next minimum of s in the direction of the nearest nucleus.) The dependence of $F_{\rm xc}$ on r_s, s, and α, i.e., many input quantities, hinders a detailed analysis. However, the overall more negative $\partial F_{\rm xc}^{\rm TASK}/\partial\alpha$ in CdO compared with NaCl can explain a larger relative contribution from the derivative discontinuity in CdO. To gain further insight, it would be of great interest to know the exact Kohn-Sham gap of CdO and see whether it indeed vanishes. QMC calculations in the spirit of Ref. [32] for CdO would therefore be of great interest.

Finally, we summarize the influence of the different bonding types on the energetically important region. In Fig. 2, we observe that for the covalently bound systems, α has a local minimum at the bond center, while in the ionic crystals α has a local maximum at the bond center. Therefore different regions of α are energetically important for the different types of bonds. On the one hand, in Ge and C the bonding region and thus values of α between 0.2 and 1 are very important. On the other hand, in NaCl and CdO the inner valence and the core-valence regions and thus values of α between 0.4 and 2 appear to be energetically most important. Figure 3 shows that the magnitude of $\partial F_{\rm xc}^{\rm TASK}/\partial\alpha$ is particularly high for α between 0.4 and 2. This underlines the importance of the construction principle, Eq. (19), and explains why TASK yields reliable band gaps for many systems.

V. THE IMPACT OF CORRELATION

While there is a lot of evidence that the total xc derivative discontinuity as well as the one of pure exact exchange should be positive, there are several hints that the contribution from correlation should typically be negative: Exact exchange typically yields a derivative discontinuity that is too large [34,77], which implies that the correlation part of the exact functional must have a negative contribution to $\Delta_{\rm xc}$. For the correlation that corresponds to the dynamical (random phase approximation) screening in the *GW* approximation, this has also been confirmed explicitly [34].

In the context of meta-GGAs, we have a further argument supporting this point of view based on the enhancement factor for fully spin-polarized systems. As shown above, the derivative discontinuity can be linked to the derivative of the enhancement factor with respect to α via Eq. (19). In the one-electron case ($\alpha = 0$), the exact correlation must vanish identically to make the correlation free from self-interaction. Since the correlation energy of the exact functional is nonpositive, we have [97] $\varepsilon_{\rm c}(\alpha = 0) \geqslant \varepsilon_{\rm c}(\alpha)$, and thus $F_{\rm c}(\alpha = 0) \leqslant F_{\rm c}(\alpha)$ for all values of α and of the remaining parameters. In particular, the correlation energy density of the homogeneous electron gas is negative everywhere, and thus $F_{\rm c}(n, \nabla n = 0, \alpha = 0) < F_{\rm c}(n, \nabla n = 0, \alpha = 1)$ for all values of the density n. Consequently, the average of $\partial F{\rm c}/\partial\alpha$ for α between 0 and 1 must be positive. Because $0 < \alpha < 1$ typically makes a large part of the energetically important region, the analog of Eq. (19) for correlation indicates $\Delta_{\rm c} < 0$.

These considerations indicate which trends are to be expected for exact exchange and exact correlation. In the construction of approximate functionals, however, one additionally has to take into account that semilocal exchange functionals do not model exact exchange, but effectively cover exchange and nondynamical correlation [75,98–103]. Therefore the relative contributions of meta-GGA exchange and meta-GGA correlation to the total derivative discontinuity may differ depending on the specific functional construction strategy, and only their sum, i.e., the total $\Delta_{\rm xc}$, is of decisive relevance. This is in line with the long-known experience that semilocal approximations for exchange (x) and correlation (c) must match and are therefore best designed together. The correlation functionals of popular meta-GGAs such as Strongly Constrained and Appropriately Normed (SCAN) [60], r2SCAN [104], and M06-L [56] have a noticeable negative contribution to the derivative discontinuity. They are therefore expected to reduce band gaps (cf. the Supplemental Material [81], where this is explicitly confirmed for SCAN). The results shown in Fig. 1 indicate that TASK exchange, which has been constructed differently from previous meta-GGAs by following the philosophy of Eq. (18), needs a different kind of correlation functional. The CC–meta-GGA correlation [82] takes this into account: While having a nonpositive derivative discontinuity in general, it preserves the high quality of the band gaps for the systems in the test set.

VI. BAND GAPS OF METAL-HALIDE PEROVSKITES

The test set studied in Sec. III provides a reasonable benchmark as it spans a broad range of materials with band gaps from large to small. While the focus of Sec. III is on the comparison of the gaps from generalized Kohn-Sham and Kohn-Sham theory, it is reassuring to know that the high quality of the generalized Kohn-Sham gaps from the TASK functional has been confirmed also for other, yet larger test sets [69]. However, from a materials science perspective, the question of how reliably DFT can predict the gaps of very complex materials is also highly relevant. For many such materials, definite reference values have not been established yet, excluding them from typical test sets. Furthermore, for some materials, predicting the band gap correctly is challenging in general, i.e., not only for DFT, but also for other many-body methods. A paradigmatic example is the material family of metal-halide perovskites, which pose a serious challenge even for Green's-function-based many-body perturbation theory in the *GW* approximation [105–108]. The *GW* approach is currently considered to be the "gold standard" for the prediction of band gaps of solids [109], but it requires material-dependent, sufficiently accurate DFT starting points [108,110] or computationally demanding (partial) self-consistency and the incorporation of vertex corrections for halide perovskites [107,111]. While the considerations

TABLE I. Kohn-Sham (for PBE) and generalized Kohn-Sham (for HSE and TASK) band gaps (in eV) calculated with the different programs VASP [113,114] and BAND [115]. The VASP values are taken from Ref. [108]; other values are from this work. See main text for details.

System	PBE VASP	PBE BAND	HSE VASP	TASK BAND	HSE BAND
$MAPbI_3$	0.21	0.09	0.82	0.81	
$MAPbBr_3$	0.55	0.41	1.30	1.38	
$CsSnBr_3$	0.06	0.01	0.63	0.73	
$(MA)_2BiTlBr_6$	0.60	0.44	1.00	1.25	
$Cs_2TlAgBr_6$	−0.66	−0.57	0.20	−0.05	0.08
$Cs_2TlAgCl_6$	0.00	0.00	1.09	0.75	1.07
$Cs_2BiAgBr_6$	1.09	1.05	1.95	1.86	
$Cs_2InAgCl_6$	1.16	1.18	2.61	2.49	2.49
Cs_2SnBr_6	1.10	1.10	2.14	2.07	
$Cs_2Au_2I_6$	0.70	0.71	1.16	0.91	

presented in the literature [56,63,69,112] and in this paper suggest that a meta-GGA such as the TASK functional is an attractive option for predicting band gaps, the question arises whether it can also predict the band gaps of metal-halide perovskites with quantitative accuracy.

The HSE screened hybrid functional [37,38] is one of the most reliable common functionals for the purposes of band-gap prediction [69]. A reasonable description of the band gaps of semiconductors has been part of its construction strategy, and HSE generalized Kohn-Sham gaps often give reasonable estimates of the true fundamental gaps. A major drawback is, however, that the Fock-like integrals that are required in an HSE calculation are computationally demanding, and especially so in plane-wave calculations, limiting the possibilities of rapid materials screening. A computationally efficient meta-GGA giving band gaps similar to the HSE functional would thus be an attractive alternative. Therefore we examine in the following whether the TASK meta-GGA can fulfill this promise by comparing TASK band gaps with HSE band gaps. Table I summarizes results for ten different metal-halide perovskites. These systems span a broad range of gaps from below 1 eV to over 2.5 eV, and a broad range of chemical complexity from single perovskites with chemical formula ABX_3 to the quaternary double perovskites with formula $A_2BB'X_6$, where A is a monovalent cation such as Cs^+ or $CH_3NH_3^+$ (MA), B and B' are metal cations, and X is a halide anion. In all cases we used experimental structures with the structural details reported in Ref. [108]. In the compounds in which A = MA, we replaced MA with Cs in our calculations to avoid spurious symmetry breaking induced by the dipole moment of the MA molecule in the primitive cubic unit cell [116,117]. This choice, as well as other technical choices, e.g., regarding pseudopotentials, basis sets, the **k** grid, and other convergence criteria, influence the calculated numbers. We report these parameters and resulting estimates of the technical accuracy of the calculations in the Supplemental Material [81].

We use the all-electron code BAND for the TASK calculations. In this way we avoid any inconsistency that would result from the fact that self-consistent pseudopotentials are not yet available for the TASK functional. On the other hand, we cannot use BAND for all HSE calculations, because in BAND, HSE via the LIBXC interface [118] is only available for calculations without spin-orbit coupling (SOC) or with scalar-relativistic SOC. Full SOC, however, plays an important role in some of the materials in Table I. Therefore, for the HSE band gaps, we rely on the Vienna *ab initio* simulation package (VASP) values reported in Ref. [108] (with self-consistent SOC) for most of the halide perovskites and double-check only the ones for which SOC plays a negligible role ($Cs_2TlAgBr_6$, $Cs_2TlAgCl_6$, and $Cs_2InAgCl_6$) with HSE in BAND. The TASK calculations with BAND use the zeroth-order regular approximation (ZORA) [89] for including SOC for all materials except the abovementioned three exceptions, for which we performed scalar-relativistic calculations.

To give an impression of the possible consequences of the technical differences between VASP and BAND, we report in the first column of Table I the PBE band gaps calculated with VASP using plane waves and projector-augmented wave pseudopotentials, and in the second column we report the PBE gaps from our calculations using BAND with an all-electron localized basis set. This comparison shows that differences of ∼0.15 eV can result just due to technical differences between the VASP calculations from Ref. [108] and the BAND calculations from this work.

With this in mind, we now compare the HSE band gaps in the third column of Table I with the TASK band gaps in the fourth column. For most systems, the values are rather close, and differences are within the ∼0.15 eV range that we already observed in the PBE comparison. However, for $MA_2BiTlBr_6$, the TASK gap is larger by 0.25 eV, and for $Cs_2TlAgBr_6$, $Cs_2Au_2I_6$, and $Cs_2TlAgCl_6$, the HSE gap is larger by 0.25, 0.25, and 0.34 eV, respectively. We therefore take a closer look at these special cases before drawing general conclusions. Among these outliers, $Cs_2TlAgBr_6$ appears particularly noteworthy, because with TASK the gap is close to zero but negative, whereas with HSE we find a gap close to zero but positive. We look into this case in more detail in order to check whether this reflects a qualitative difference between the two xc approximations, or just sensitivity to the computational details. To this end, we repeated the HSE calculation for $Cs_2TlAgBr_6$ using BAND. This is possible because SOC plays a minor role here, as discussed above. The corresponding number is shown in the fifth column of Table I. With BAND, the HSE gap of $Cs_2TlAgBr_6$ is 0.12 eV smaller than with VASP. As a further test we also calculated the band gap of $Cs_2TlAgBr_6$ using the TASK functional in QUANTUM ESPRESSO (QE) [122,123], i.e., another plane-wave code. In QE, the TASK gap of $Cs_2TlAgBr_6$ is 0.04 eV, i.e., small but positive. Both results show that technical differences play a major role for the sign of the band gap in this system, and we conclude that $Cs_2TlAgBr_6$ does not reveal a qualitative difference between HSE and TASK; however, the gap is so close to zero in either case that technical differences can be decisive for whether the gap is slightly positive or slightly negative.

For the sake of completeness we also calculated the band gaps of the other two materials for which full SOC does not play a role with HSE in BAND. The corresponding numbers in the fifth column of Table I show that TASK and

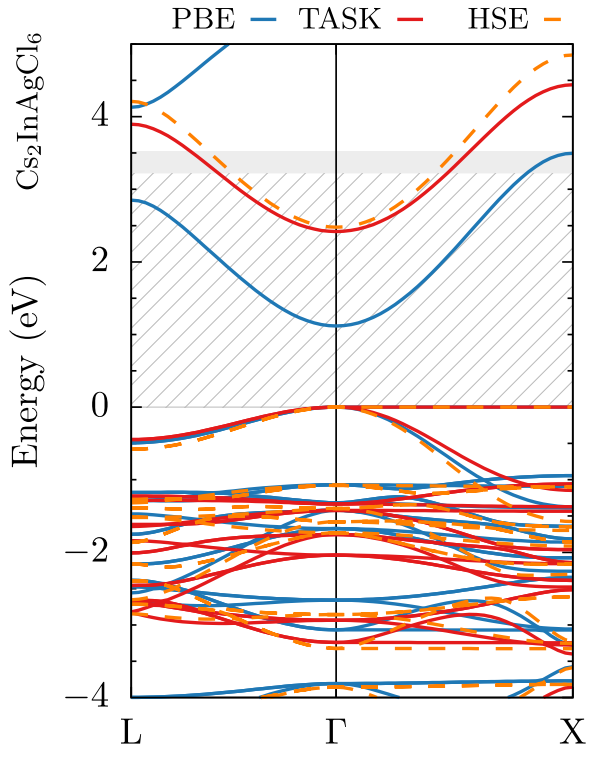

FIG. 4. PBE, HSE, and TASK band structures as calculated with BAND for $Cs_2InAgCl_6$. Not only the gaps, but also the band structures are rather similar for HSE and TASK. The hatched and shaded regions indicate experimental values for the band gap, with the hatched region indicating the gap, and the shaded region indicating the range from different experiments [119–121].

HSE yield identical gaps for $Cs_2InAgCl_6$ with BAND, and for $Cs_2TlAgCl_6$ the difference between HSE and TASK is slightly reduced when the functionals are compared within BAND. As a further check, we compared not only the gaps, but also the band structures. Figure 4 shows the comparison for the exemplary case of $Cs_2InAgCl_6$. The band structures obtained with TASK and HSE are very similar, with slight differences in the dispersion of the conduction band at the *L* and *X* points.

In summary, we therefore conclude that the band gaps obtained from HSE and TASK are not identical, but close to each other. Both functionals seem to capture the band structure physics of complex metal-halide perovskite materials in a similar way. This finding suggests that instead of basing band structure estimates on the nonlocal, screened hybrid functional HSE, one may as well use the meta-GGA TASK for these purposes. Our findings also suggest that the TASK functional may be an attractive starting point for a subsequent *GW* calculation.

The reason for why this is is an attractive option from a computational perspective is summarized in Table II. It shows the computational time required for an HSE and a TASK calculation for each of the three metal-halide perovskites for which SOC plays a minor role and which therefore can reasonably be compared within BAND. The most relevant column is the last one. It reports the time relative to a PBE calculation with the same computational settings for a complete calculation with the given xc functional. By reporting these relative values, Table II provides an impression of the computational expense independent of the specific hardware that we used. For the sake of transparency and completeness, we further report the hardware and absolute timings. The numbers reveal that a calculation using TASK takes about three times as long as the PBE calculation, whereas an HSE calculation can take more than a factor of 90 longer than the PBE calculation. Using TASK instead of HSE typically saves a factor of about 25 in computational time. As a relevant side note we point out that calculations with TASK do not require a finer numerical grid than the PBE calculations. Many program packages have default settings that use an extra fine radial grid ("grid

TABLE II. Computational time required for a self-consistent field (SCF) calculation with PBE, TASK, and HSE with BAND including the sampling of the band structure. The last column reports the compute time of HSE and TASK relative to a PBE calculation. For completeness, the prior columns report absolute numbers obtained on a compute node with two CPUs of type Intel Xeon E5-2630 v4 at 2.20 GHz (Broadwell) with 2 × 32 GB RAM (in total 20 physical cores, hyperthreading enabled) using a 4 × 4 × 4 **k** grid, without a frozen core, normal numerical quality, and disabled symmetry and including scalar relativistic effects in the ZORA. Note that the TASK calculations do *not* require the grid boost, which many programs switch on as a default for meta-GGAs. DZ and TZP denote double-zeta and triple-zeta polarized basis sets, respectively.

				CPU time (s)		CPU time relative to PBE (s)	
System	xc	Basis	Grid boost	SCF step	Total	SCF step	Total
$Cs_2TlAgCl_6$	PBE	TZP	✗	45	1021	1.00	1.00
$Cs_2TlAgCl_6$	TASK	TZP	✗	140	2969	3.11	2.88
$Cs_2TlAgCl_6$	TASK	TZP	√	324	6890	7.20	6.75
$Cs_2TlAgCl_6$	HSE	TZP	✗	4560	78699	106.05	77.09
$Cs_2TlAgBr_6$	PBE	DZ	✗	25	561	1.00	1.00
$Cs_2TlAgBr_6$	TASK	DZ	✗	106	2170	4.24	3.87
$Cs_2TlAgBr_6$	TASK	DZ	√	258	5153	10.32	9.18
$Cs_2TlAgBr_6$	HSE	DZ	✗	2867	53006	114.68	94.47
$Cs_2InAgCl_6$	PBE	DZ	✗	13	453	1.00	1.00
$Cs_2InAgCl_6$	TASK	DZ	✗	56	1268	4.31	2.80
$Cs_2InAgCl_6$	TASK	DZ	√	141	2913	10.85	6.43
$Cs_2InAgCl_6$	HSE	DZ	✗	1320	23518	101.54	51.91

boost") in meta-GGA calculations, because meta-GGAs such as SCAN and M06-L require a fine grid due to their numerical sensitivity. TASK calculations, however, converge well to the proper values on the regular grid. Therefore the grid boost, which typically more than doubles computational times, can be disabled.

We thus arrive at the final important finding of this paper: The TASK meta-GGA functional that only requires semilocal orbital input predicts band gaps similar to the ones from the fully nonlocal screened hybrid HSE, but at much lower computational cost—in the cases that we studied typically lower by a factor of 25.

Finally, we briefly comment on the comparison with experimental band gaps, which is particularly challenging for complex materials such as the metal-halide perovskites for which the range of experimentally reported band gaps can be substantial. While the focus of our paper is not on the comparison with experiment, it is worth noting that for some systems, e.g., $Cs_2BiAgBr_6$, the gaps calculated with HSE and TASK are close to the measured gaps, while for others the difference can be as large as ∼0.8 eV, e.g., for $MAPbI_3$ and $Cs_2InAgCl_6$; cf. Fig. 4. These differences are generally in line with observations from molecular-dynamics simulations showing that anharmonic structural fluctuations at elevated temperatures can lead to a significant renormalization of the band gap [107,124,125], reported to be as large as 0.7 eV for some halide perovskites [107]. Furthermore, exciton binding energies of some metal-halide perovskites are of the order of several hundred meV [126], and orbital symmetries can lead to parity-forbidden transitions [127,128]. This further complicates the comparison with experimentally measured band gaps, which are typically extracted from optical absorption measurements. A detailed, benchmarklike comparison of theory and experiment is therefore challenging for the broad family of metal-halide perovskites. Nevertheless, in itself and as a starting point for subsequent *GW* calculations, it is a promising finding for computational materials science that the TASK meta-GGA allows for a qualitatively reasonable prediction of the gap similar to HSE at much reduced computational cost.

VII. SUMMARY AND CONCLUSIONS

In summary, we have shown why and how meta-GGAs can predict the right band gaps of solids for the right reason by generating a sizable derivative discontinuity. This demonstrates that meta-GGAs can provide accurate band gaps at semilocal computational cost without suffering from the shortcomings that other semilocal methods have. By comparing calculations within the Kohn-Sham scheme and the generalized Kohn-Sham scheme for the TASK functional, we have demonstrated how the construction principle $\partial e_{xc}/\partial\tau > 0$, which corresponds to $\partial F_{xc}/\partial\alpha < 0$, is crucial for the derivative discontinuity and thus the nonlocality of a meta-GGA. We further argued that the contribution that correlation makes to the derivative discontinuity should generally be negative, and that the relative magnitude of the contributions from exchange and correlation for semilocal functionals may depend on the specific construction principles that are used. In addition to a test set of well-studied solids for which TASK yields band gaps close to the experimentally measured ones, we have also investigated a set of ten metal-halide perovskites for which the band gaps are notoriously difficult to predict. We have shown that for these systems, the band gaps found with TASK are close to the band gaps that one finds with HSE; yet the computational cost of the TASK calculation is lower by a factor of about 25. The combination of reasonable accuracy and numerical efficiency thus makes the TASK meta-GGA a natural choice for computationally efficient first-principles band-gap screening.

All authors together conceptualized the work. T.L. performed the calculations reported in Secs. III, IV, and V and wrote the required routines. T.A. performed the calculations reported in Sec. VI and wrote the required routines. T.L. and S.K. wrote the manuscript, and all authors discussed the final version.

ACKNOWLEDGMENTS

S.K. and T.L. appreciate financial support from the Deutsche Forschungsgemeinschaft, DFG Project No. KU 1410/4-1, and from the Bavarian State Ministry of Science, Research, and the Arts for the Collaborative Research Network "Solar Technologies go Hybrid." L.L. acknowledges funding from the Dutch Research Council (NWO) under Grant No. OCENW.M20.337. S.K. and T.L. are further grateful for support from the Elite Study Program "Biological Physics" of the Elite Network of Bavaria, and T.L. acknowledges discussions with Pier Philippsen on generating data for plots with BAND. J.S. acknowledges the support of the U.S. DOE, Office of Science, Basic Energy Sciences Grant No. DE-SC0019350.

[1] G. Ceder, Opportunities and challenges for first-principles materials design and applications to Li battery materials, MRS Bull. **35**, 693 (2010).

[2] I. E. Castelli, T. Olsen, S. Datta, D. D. Landis, S. Dahl, K. S. Thygesen, and K. W. Jacobsen, Computational screening of perovskite metal oxides for optimal solar light capture, Energy Environ. Sci. **5**, 5814 (2012).

[3] J. Kang, X. Zhang, and S.-H. Wei, Advances and challenges in DFT-based energy materials design, Chin. Phys. B **31**, 107105 (2022).

[4] X. Ye, A. Liu, L. Gao, C. Zhang, L. Yan, S. Wen, and T. Ma, Computational screening of Cs based vacancy-ordered double perovskites for solar cell and photocatalysis applications, EcoMat **5**, e12295 (2023).

[5] Q. Wu, M. Pan, S. Zhang, D. Sun, Y. Yang, D. Chen, D. A. Weitz, and X. Gao, Research progress in high-throughput screening of CO_2 reduction catalysts, Energies **15**, 6666 (2022).

[6] Q. He, B. Yu, Z. Li, and Y. Zhao, Density functional theory for battery materials, Energy Environ. Mater. **2**, 264 (2019).

[7] L. Kahle, A. Marcolongo, and N. Marzari, High-throughput computational screening for solid-state Li-ion conductors, Energy Environ. Sci. **13**, 928 (2020).

[8] A. Jain, S. P. Ong, G. Hautier, W. Chen, W. D. Richards, S. Dacek, S. Cholia, D. Gunter, D. Skinner, G. Ceder, and K. A. Persson, Commentary: The Materials Project: A materials genome approach to accelerating materials innovation, APL Mater. **1**, 011002 (2013).

[9] Y. Kang, Y. Youn, S. Han, J. Park, and C.-S. Oh, Computational screening of indirect-gap semiconductors for potential photovoltaic absorbers, Chem. Mater. **31**, 4072 (2019).

[10] C. C. Stoumpos, D. H. Cao, D. J. Clark, J. Young, J. M. Rondinelli, J. I. Jang, J. T. Hupp, and M. G. Kanatzidis, Ruddlesden-Popper hybrid lead iodide perovskite 2D homologous semiconductors, Chem. Mater. **28**, 2852 (2016).

[11] B. Saparov and D. B. Mitzi, Organic–inorganic perovskites: Structural versatility for functional materials design, Chem. Rev. **116**, 4558 (2016).

[12] M. D. Smith, E. J. Crace, A. Jaffe, and H. I. Karunadasa, The diversity of layered halide perovskites, Annu. Rev. Mater. Res. **48**, 111 (2018).

[13] N. R. Wolf, B. A. Connor, A. H. Slavney, and H. I. Karunadasa, Doubling the stakes: The promise of halide double perovskites, Angew. Chem. Int. Ed. **60**, 16264 (2021).

[14] National Renewable Energy Laboratory, Best research-cell efficiencies, https://www.nrel.gov/pv/assets/images/efficiency-chart.png.

[15] F. A. Faber, A. Lindmaa, O. A. von Lilienfeld, and R. Armiento, Machine Learning Energies of 2 Million Elpasolite (ABC_2D_6) Crystals, Phys. Rev. Lett. **117**, 135502 (2016).

[16] M. R. Filip and F. Giustino, The geometric blueprint of perovskites, Proc. Natl. Acad. Sci. USA **115**, 5397 (2018).

[17] W. Shockley and H. J. Queisser, Detailed balance limit of efficiency of *p-n* junction solar cells, J. Appl. Phys. **32**, 510 (1961).

[18] J. P. Perdew and M. Levy, Physical Content of the Exact Kohn-Sham Orbital Energies: Band Gaps and Derivative Discontinuities, Phys. Rev. Lett. **51**, 1884 (1983).

[19] L. J. Sham and M. Schlüter, Density-Functional Theory of the Energy Gap, Phys. Rev. Lett. **51**, 1888 (1983).

[20] J. P. Perdew, R. G. Parr, M. Levy, and J. L. Balduz, Jr., Density-Functional Theory for Fractional Particle Number: Derivative Discontinuities of the Energy, Phys. Rev. Lett. **49**, 1691 (1982).

[21] With periodic boundary conditions, one can distinguish between a direct and an indirect one-electron gap, and for a chosen band occupation, the indirect gap can be negative.

[22] J. P. Perdew, Density functional theory and the band gap problem, Int. J. Quantum Chem. **28**, 497 (1985).

[23] A. J. Cohen, P. Mori-Sánchez, and W. Yang, Fractional charge perspective on the band gap in density-functional theory, Phys. Rev. B **77**, 115123 (2008).

[24] P. Mori-Sánchez, A. J. Cohen, and W. Yang, Localization and Delocalization Errors in Density Functional Theory and Implications for Band-Gap Prediction, Phys. Rev. Lett. **100**, 146401 (2008).

[25] P. Mori-Sánchez, A. J. Cohen, and W. Yang, Discontinuous Nature of the Exchange-Correlation Functional in Strongly Correlated Systems, Phys. Rev. Lett. **102**, 066403 (2009).

[26] W. Yang, A. J. Cohen, and P. Mori-Sanchez, Derivative discontinuity, bandgap and lowest unoccupied molecular orbital in density functional theory, J. Chem. Phys. **136**, 204111 (2012).

[27] W. Kohn and L. J. Sham, Self-consistent equations including exchange and correlation effects, Phys. Rev. **140**, A1133 (1965).

[28] A. D. Becke, Density-functional exchange-energy approximation with correct asymptotic behavior, Phys. Rev. A **38**, 3098 (1988).

[29] J. P. Perdew, K. Burke, and M. Ernzerhof, Generalized Gradient Approximation Made Simple, Phys. Rev. Lett. **77**, 3865 (1996).

[30] R. W. Godby, M. Schlüter, and L. J. Sham, Self-energy operators and exchange-correlation potentials in semiconductors, Phys. Rev. B **37**, 10159 (1988).

[31] G. Onida, L. Reining, and A. Rubio, Electronic excitations: Density-functional versus many-body Green's-function approaches, Rev. Mod. Phys. **74**, 601 (2002).

[32] A. Aouina, M. Gatti, S. Chen, S. Zhang, and L. Reining, Accurate Kohn-Sham auxiliary system from the ground state density of solids, Phys. Rev. B **107**, 195123 (2023).

[33] R. W. Godby, M. Schlüter, and L. J. Sham, Accurate Exchange-Correlation Potential for Silicon and Its Discontinuity on Addition of an Electron, Phys. Rev. Lett. **56**, 2415 (1986).

[34] M. Grüning, A. Marini, and A. Rubio, Density functionals from many-body perturbation theory: The band gap for semiconductors and insulators, J. Chem. Phys. **124**, 154108 (2006).

[35] M. Grüning, A. Marini, and A. Rubio, Effect of spatial nonlocality on the density functional band gap, Phys. Rev. B **74**, 161103(R) (2006).

[36] A. Seidl, A. Görling, P. Vogl, J. A. Majewski, and M. Levy, Generalized Kohn-Sham schemes and the band-gap problem, Phys. Rev. B **53**, 3764 (1996).

[37] J. Heyd, G. E. Scuseria, and M. Ernzerhof, Hybrid functionals based on a screened Coulomb potential, J. Chem. Phys. **118**, 8207 (2003); **124**, 219906(E) (2006).

[38] A. V. Krukau, O. A. Vydrov, A. F. Izmaylov, and G. E. Scuseria, Influence of the exchange screening parameter on the performance of screened hybrid functionals, J. Chem. Phys. **125**, 224106 (2006).

[39] L. Kronik, T. Stein, S. Refaely-Abramson, and R. Baer, Excitation gaps of finite-sized systems from optimally tuned range-separated hybrid functionals, J. Chem. Theory Comput. **8**, 1515 (2012).

[40] L. Kronik and S. Kümmel, Dielectric screening meets optimally tuned density functionals, Adv. Mater. **30**, 1706560 (2018).

[41] J. F. Janak, Proof that $\frac{\partial E}{\partial n_i} = \varepsilon$ in density-functional theory, Phys. Rev. B, **18**, 7165 (1978).

[42] T. Stein, J. Autschbach, N. Govind, L. Kronik, and R. Baer, Curvature and frontier orbital energies in density functional theory, J. Phys. Chem. Lett. **3**, 3740 (2012).

[43] D. Wing, J. B. Haberb, M. R. Filipd, S. E. Gantb, J. B. Neaton, G. Ohadaand, and L. Kronik, Band gaps of crystalline solids from Wannier-localization–based optimal tuning of a screened range-separated hybrid functional, Proc. Natl. Acad. Sci. USA **118**, e2104556118 (2021).

[44] S. Kümmel and J. P. Perdew, Optimized effective potential made simple: Orbital functionals, orbital shifts, and the exact Kohn-Sham exchange potential, Phys. Rev. B **68**, 035103 (2003).

[45] F. Tran and P. Blaha, Accurate Band Gaps of Semiconductors and Insulators with a Semilocal Exchange-Correlation Potential, Phys. Rev. Lett. **102**, 226401 (2009).
[46] R. Armiento and S. Kümmel, Orbital Localization, Charge Transfer, and Band Gaps in Semilocal Density-Functional Theory, Phys. Rev. Lett. **111**, 036402 (2013).
[47] T. Aschebrock, R. Armiento, and S. Kümmel, Orbital nodal surfaces: Topological challenges for density functionals, Phys. Rev. B **95**, 245118 (2017).
[48] T. Aschebrock, R. Armiento, and S. Kümmel, Challenges for semilocal density functionals with asymptotically nonvanishing potentials, Phys. Rev. B **96**, 075140 (2017).
[49] D. Waroquiers, A. Lherbier, A. Miglio, M. Stankovski, S. Poncé, M. J. T. Oliveira, M. Giantomassi, G.-M. Rignanese, and X. Gonze, Band widths and gaps from the Tran-Blaha functional: Comparison with many-body perturbation theory, Phys. Rev. B **87**, 075121 (2013).
[50] A. Lindmaa and R. Armiento, Energetics of the AK13 semilocal Kohn-Sham exchange energy functional, Phys. Rev. B **94**, 155143 (2016).
[51] J. Camargo-Martínez and R. Baquero, Performance of the modified Becke-Johnson potential for semiconductors, Phys. Rev. B **86**, 195106 (2012).
[52] A. D. Becke, Density-functional thermochemistry. IV. A new dynamical correlation functional and implications for exact-exchange mixing, J. Chem. Phys. **104**, 1040 (1996).
[53] T. Van Voorhis and G. E. Scuseria, A novel form for the exchange-correlation energy functional, J. Chem. Phys. **109**, 400 (1998).
[54] A. D. Boese and N. C. Handy, New exchange-correlation density functionals: The role of the kinetic-energy density, J. Chem. Phys. **116**, 9559 (2002).
[55] J. Tao, J. P. Perdew, V. N. Staroverov, and G. E. Scuseria, Climbing the Density Functional Ladder: Nonempirical Meta–Generalized Gradient Approximation Designed for Molecules and Solids, Phys. Rev. Lett. **91**, 146401 (2003).
[56] Y. Zhao and D. G. Truhlar, A new local density functional for main-group thermochemistry, transition metal bonding, thermochemical kinetics, and noncovalent interactions, J. Chem. Phys. **125**, 194101 (2006).
[57] J. Sun, B. Xiao, and A. Ruzsinszky, Communication: Effect of the orbital-overlap dependence in the meta generalized gradient approximation, J. Chem. Phys. **137**, 051101 (2012).
[58] R. Peverati and D. G. Truhlar, An improved and broadly accurate local approximation to the exchange–correlation density functional: The MN12-L functional for electronic structure calculations in chemistry and physics, Phys. Chem. Chem. Phys. **14**, 13171 (2012).
[59] J. Sun, R. Haunschild, B. Xiao, I. W. Bulik, G. E. Scuseria, and J. P. Perdew, Semilocal and hybrid meta-generalized gradient approximations based on the understanding of the kinetic-energy-density dependence, J. Chem. Phys. **138**, 044113 (2013).
[60] J. Sun, A. Ruzsinszky, and J. P. Perdew, Strongly Constrained and Appropriately Normed Semilocal Density Functional, Phys. Rev. Lett. **115**, 036402 (2015).
[61] T. Aschebrock and S. Kümmel, Ultranonlocality and accurate band gaps from a meta-generalized gradient approximation, Phys. Rev. Res. **1**, 033082 (2019).
[62] F. G. Eich and M. Hellgren, Derivative discontinuity and exchange-correlation potential of meta-GGAs in density-functional theory, J. Chem. Phys. **141**, 224107 (2014).
[63] Z. H. Yang, H. Peng, J. Sun, and J. P. Perdew, More realistic band gaps from meta-generalized gradient approximations: Only in a generalized Kohn-Sham scheme, Phys. Rev. B **93**, 205205 (2016).
[64] J. P. Perdew, W. Yang, K. Burke, Z. Yang, E. K. U. Gross, M. Scheffler, G. E. Scuseria, T. M. Henderson, I. Y. Zhang, A. Ruzsinszky, H. Peng, J. Sun, E. Trushin, and A. Görling, Understanding band gaps of solids in generalized Kohn–Sham theory, Proc. Natl. Acad. Sci. USA **114**, 2801 (2017).
[65] V. U. Nazarov and G. Vignale, Optics of Semiconductors from Meta-Generalized-Gradient-Approximation-Based Time-Dependent Density-Functional Theory, Phys. Rev. Lett. **107**, 216402 (2011).
[66] J. Heyd, J. E. Peralta, G. E. Scuseria, and R. L. Martin, Energy band gaps and lattice parameters evaluated with the Heyd-Scuseria-Ernzerhof screened hybrid functional, J. Chem. Phys. **123**, 174101 (2005).
[67] M. K. Y. Chan and G. Ceder, Efficient Band Gap Prediction for Solids, Phys. Rev. Lett. **105**, 196403 (2010).
[68] B. Patra, S. Jana, L. A. Constantin, and P. Samal, Relevance of the Pauli kinetic energy density for semilocal functionals, Phys. Rev. B **100**, 155140 (2019).
[69] P. Borlido, J. Schmidt, A. Huran, F. Tran, M. Marques, and S. Botti, Exchange-correlation functionals for band gaps of solids: Benchmark, reparametrization and machine learning, npj Comput. Mater. **6**, 96 (2020).
[70] P. Kovács, F. Tran, P. Blaha, and G. K. Madsen, What is the optimal mGGA exchange functional for solids? J. Chem. Phys. **157**, 094110 (2022).
[71] In the literature, functionals that depend on the Laplacian of the density are also labeled meta-GGAs. In this paper, however, we consider functionals that must depend on the kinetic energy density and may depend on the Laplacian of the density, since the nonlocality in meta-GGAs is fully due to their orbital dependence.
[72] E. R. Johnson, S. Keinan, P. Mori-Sánchez, J. Contreras-García, A. J. Cohen, and W. Yang, Revealing noncovalent interactions, J. Am. Chem. Soc. **132**, 6498 (2010).
[73] J. Sun, B. Xiao, Y. Fang, R. Haunschild, P. Hao, A. Ruzsinszky, G. I. Csonka, G. E. Scuseria, and J. P. Perdew, Density Functionals that Recognize Covalent, Metallic, and Weak Bonds, Phys. Rev. Lett. **111**, 106401 (2013).
[74] G. L. Oliver and J. P. Perdew, Spin-density gradient expansion for the kinetic energy, Phys. Rev. A **20**, 397 (1979).
[75] S. Kümmel and L. Kronik, Orbital-dependent density functionals: Theory and applications, Rev. Mod. Phys. **80**, 3 (2008).
[76] G. K.-L. Chan, A fresh look at ensembles: Derivative discontinuities in density functional theory, J. Chem. Phys. **110**, 4710 (1999).
[77] M. Städele, M. Moukara, J. A. Majewski, P. Vogl, and A. Görling, Exact exchange Kohn-Sham formalism applied to semiconductors, Phys. Rev. B **59**, 10031 (1999).
[78] M. J. Allen and D. J. Tozer, Eigenvalues, integer discontinuities and NMR shielding constants in Kohn-Sham theory, Mol. Phys. **100**, 433 (2002).

[79] M. Mundt and S. Kümmel, Derivative Discontinuities in Time-Dependent Density-Functional Theory, Phys. Rev. Lett. **95**, 203004 (2005).
[80] M. Lein and S. Kümmel, Exact Time-Dependent Exchange-Correlation Potentials for Strong-Field Electron Dynamics, Phys. Rev. Lett. **94**, 143003 (2005).
[81] See Supplemental Material at http://link.aps.org/supplemental/10.1103/PhysRevMaterials.7.093803 for details on the numerical parameters used and detailed data.
[82] T. Lebeda, T. Aschebrock, and S. Kümmel, First steps towards achieving both ultranonlocality and a reliable description of electronic binding in a meta-generalized gradient approximation, Phys. Rev. Res. **4**, 023061 (2022).
[83] J. P. Perdew and Y. Wang, Accurate and simple analytic representation of the electron-gas correlation energy, Phys. Rev. B **45**, 13244 (1992).
[84] Alternatively, one could calculate Δ_x directly in the OEP formalism [75,77,92], but the generalized Kohn-Sham calculation is technically more straightforward.
[85] G. te Velde and E. J. Baerends, Precise density-functional method for periodic structures, Phys. Rev. B **44**, 7888 (1991).
[86] G. Wiesenekker and E. J. Baerends, Quadratic integration over the three-dimensional Brillouin zone, J. Phys.: Condens. Matter **3**, 6721 (1991).
[87] M. Franchini, P. H. T. Philipsen, and L. Visscher, The Becke fuzzy cells integration scheme in the Amsterdam density functional program suite, J. Comput. Chem. **34**, 1819 (2013).
[88] M. Franchini, P. H. T. Philipsen, E. van Lenthe, and L. Visscher, Accurate Coulomb potentials for periodic and molecular systems through density fitting, J. Chem. Theory Comput. **10**, 1994 (2014).
[89] E. van Lenthe, E.-J. Baerends, and J. G. Snijders, Relativistic regular two-component Hamiltonians, J. Chem. Phys. **99**, 4597 (1993).
[90] E. Van Lenthe and E. J. Baerends, Optimized Slater-type basis sets for the elements 1–118, J. Comput. Chem. **24**, 1142 (2003).
[91] SCM, Theoretical Chemistry, Vrije Universiteit, BAND 2022.1, https://www.scm.com/; note that a modified version is used in this paper.
[92] J. B. Krieger, Y. Li, and G. J. Iafrate, Construction and application of an accurate local spin-polarized Kohn-Sham potential with integer discontinuity: Exchange-only theory, Phys. Rev. A **45**, 101 (1992).
[93] S. Lehtola and M. A. Marques, Many recent density functionals are numerically ill-behaved, J. Chem. Phys. **157**, 174114 (2022).
[94] S. Lehtola, Meta-GGA density functional calculations on atoms with spherically symmetric densities in the finite element formalism, J. Chem. Theory Comput. **19**, 2502 (2023).
[95] S. Lehtola, Atomic electronic structure calculations with Hermite interpolating polynomials, J. Phys. Chem. A **127**, 4180 (2023).
[96] In Ref. [93], the numerical problems of other meta-GGAs are attributed to the use of the iso-orbital indicator α. However, α is also used in TASK. Therefore the numerical stability of TASK suggests that numerically stable density functional approximations can be constructed using α.
[97] Strictly speaking, this only implies $E_c \leqslant 0$. In practical approximations, however, typically $\varepsilon_c \leqslant 0$ also holds.
[98] A. D. Becke, Density-functional thermochemistry. III. The role of exact exchange, J. Chem. Phys. **98**, 5648 (1993).
[99] R. Neumann, R. H. Nobes, and N. Handy, Exchange functionals and potentials, Mol. Phys. **87**, 1 (1996).
[100] D. K. W. Mok, R. Neumann, and N. C. Handy, Dynamical and nondynamical correlation, J. Phys. Chem. **100**, 6225 (1996).
[101] K. Burke, J. P. Perdew, and M. Ernzerhof, Why the generalized gradient approximation works and how to go beyond it.
[102] O. Gritsenko, P. Schipper, and E. Baerends, Exchange and correlation energy in density functional theory: Comparison of accurate DFT quantities with traditional Hartree–Fock based ones and generalized gradient approximations for the molecules Li_2, N_2, F_2, J. Chem. Phys. **107**, 5007 (1997).
[103] D. Cremer, Density functional theory: coverage of dynamic and non-dynamic electron correlation effects, Mol. Phys. **99**, 1899 (2001).
[104] J. W. Furness, A. D. Kaplan, J. Ning, J. P. Perdew, and J. Sun, Accurate and numerically efficient r^2SCAN meta-generalized gradient approximation, J. Phys. Chem. Lett. **11**, 8208 (2020).
[105] M. R. Filip and F. Giustino, *GW* quasiparticle band gap of the hybrid organic-inorganic perovskite $CH_3NH_3PbI_3$: Effect of spin-orbit interaction, semicore electrons, and self-consistency, Phys. Rev. B **90**, 245145 (2014).
[106] P. Scherpelz, M. Govoni, I. Hamada, and G. Galli, Implementation and validation of fully relativistic *GW* calculations: Spin-orbit coupling in molecules, nanocrystals, and solids, J. Chem. Theory Comput. **12**, 3523 (2016).
[107] J. Wiktor, U. Rothlisberger, and A. Pasquarello, Predictive determination of band gaps of inorganic halide perovskites, J. Phys. Chem. Lett. **8**, 5507 (2017).
[108] L. Leppert, T. Rangel, and J. B. Neaton, Towards predictive band gaps for halide perovskites: Lessons from one-shot and eigenvalue self-consistent *GW*, Phys. Rev. Mater. **3**, 103803 (2019).
[109] D. Golze, M. Dvorak, and P. Rinke, The *GW* compendium: A practical guide to theoretical photoemission spectroscopy, Front. Chem. **7**, 377 (2019).
[110] S. E. Gant, J. B. Haber, M. R. Filip, F. Sagredo, D. Wing, G. Ohad, L. Kronik, and J. B. Neaton, Optimally tuned starting point for single-shot *GW* calculations of solids, Phys. Rev. Mater. **6**, 053802 (2022).
[111] F. Brivio, K. T. Butler, A. Walsh, and M. van Schilfgaarde, Relativistic quasiparticle self-consistent electronic structure of hybrid halide perovskite photovoltaic absorbers, Phys. Rev. B **89**, 155204 (2014).
[112] B. Patra, S. Jana, L. A. Constantin, and P. Samal, Efficient band gap prediction of semiconductors and insulators from a semilocal exchange-correlation functional, Phys. Rev. B **100**, 045147 (2019).
[113] G. Kresse and J. Hafner, Norm-conserving and ultrasoft pseudopotentials for first-row and transition elements, J. Phys.: Condens. Matter **6**, 8245 (1994).
[114] G. Kresse and J. Furthmüller, Efficient iterative schemes for *ab initio* total-energy calculations using a plane-wave basis set, Phys. Rev. B **54**, 11169 (1996).
[115] SCM, Theoretical Chemistry, Vrije Universiteit, BAND 2017, https://www.scm.com/.

[116] L. Leppert, S. E. Reyes-Lillo, and J. B. Neaton, Electric field and strain induced Rashba effect in hybrid halide perovskites, J. Phys. Chem. Lett. **7**, 3683 (2016).

[117] K. Frohna, T. Deshpande, J. Harter, W. Peng, B. A. Barker, J. B. Neaton, S. G. Louie, O. M. Bakr, D. Hsieh, and M. Bernardi, Inversion symmetry and bulk Rashba effect in methylammonium lead iodide perovskite single crystals, Nat. Commun. **9**, 1829 (2018).

[118] S. Lehtola, C. Steigemann, M. J. Oliveira, and M. A. Marques, Recent developments in LIBXC—A comprehensive library of functionals for density functional theory, SoftwareX **7**, 1 (2018).

[119] G. Volonakis, A. A. Haghighirad, R. L. Milot, W. H. Sio, M. R. Filip, B. Wenger, M. B. Johnston, L. M. Herz, H. J. Snaith, and F. Giustino, $Cs_2InAgCl_6$: A new lead-free halide double perovskite with direct band gap, J. Phys. Chem. Lett. **8**, 772 (2017).

[120] J. Zhou, Z. Xia, M. S. Molokeev, X. Zhang, D. Peng, and Q. Liu, Composition design, optical gap and stability investigations of lead-free halide double perovskite $Cs_2AgInCl_6$, J. Mater. Chem. A **5**, 15031 (2017).

[121] T. T. Tran, J. R. Panella, J. R. Chamorro, J. R. Morey, and T. M. McQueen, Designing indirect–direct bandgap transitions in double perovskites, Mater. Horiz. **4**, 688 (2017).

[122] P. Giannozzi, S. Baroni, N. Bonini, M. Calandra, R. Car, C. Cavazzoni, D. Ceresoli, G. L. Chiarotti, M. Cococcioni, I. Dabo, A. D. Corso, S. Fabris, G. Fratesi, S. de Gironcoli, R. Gebauer, U. Gerstmann, C. Gougoussis, A. Kokalj, M. Lazzeri, L. Martin-Samos *et al.*, QUANTUM ESPRESSO: A modular and open-source software project for quantum simulations of materials, J. Phys.: Condens. Matter **21**, 395502 (2009).

[123] P. Giannozzi, Jr., O. Andreussi, T. Brumme, O. Bunau, M. B. Nardelli, M. Calandra, R. Car, C. Cavazzoni, D. Ceresoli, M. Cococcioni, N. Colonna, I. Carnimeo, A. D. Corso, S. de Gironcoli, P. Delugas, R. A. DiStasio, Jr., A. Ferretti, A. Floris, G. Fratesi, G. Fugallo *et al.*, Advanced capabilities for materials modelling with quantum espresso, J. Phys.: Condens. Matter **29**, 465901 (2017).

[124] X. G. Zhao, Z. Wang, O. I. Malyi, and A. Zunger, Effect of static local distortions vs dynamic motions on the stability and band gaps of cubic oxide and halide perovskites, Mater. Today **49**, 107 (2021).

[125] S. A. Seidl, X. Zhu, G. Reuveni, S. Aharon, C. Gehrmann, S. Caicedo-Dávila, O. Yaffe, and D. A. Egger, Anharmonic fluctuations govern the band gap of halide perovskites, Phys. Rev. Mater. **7**, L092401 (2023).

[126] R. I. Biega, M. R. Filip, L. Leppert, and J. B. Neaton, Chemically localized resonant excitons in silver-pnictogen halide double perovskites, J. Phys. Chem. Lett. **12**, 2057 (2021).

[127] A. H. Slavney, B. A. Connor, L. Leppert, and H. I. Karunadasa, A pencil-and-paper method for elucidating halide double perovskite band structures, Chem. Sci. **10**, 11041 (2019).

[128] W. Meng, X. Wang, Z. Xiao, J. Wang, D. B. Mitzi, and Y. Yan, Parity-forbidden transitions and their impacts on the optical absorption properties of lead-free metal halide perovskites and double perovskites, J. Phys. Chem. Lett. **8**, 2999 (2017).